IEEE Access
Multidisciplinary | Rapid Review | Open Access Journal

Received September 19, 2019, accepted November 12, 2019, date of publication November 25, 2019,
date of current version December 6, 2019.

Digital Object Identifier 10.1109/ACCESS.2019.2955510

Region Growing Algorithm Combined With Fast Peak Detection for Segmenting Colloidal Gold Immunochromatographic Strip Images

WENSHENG GUO[1], YUE ZHANG[2], XIAOYAN HU[1], TING ZHANG[3], MING LIANG[3], XIANGLIANG YANG[1], AND HAI YANG[1]

[1]National Engineering Research Center for Nanomedicine, College of Life Science and Technology, Huazhong University of Science and Technology, Wuhan 430074, China
[2]School of Engineering Sciences, Wuhan National Laboratory for Optoelectronics, Huazhong University of Science and Technology, Wuhan 430074, China
[3]Research and Development Center, Infinitus (China) Company Ltd., Guangzhou 510663, China

Corresponding author: Hai Yang (yanghai@hust.edu.cn)

This work was supported in part by the National Basic Research Program of China under Grant 2015CB931802, in part by the National Science Foundation of China under Grant 81771978, and in part by the PCSIRT under Grant IRT13016.

ABSTRACT Accurate segmentation of test line and control line for colloidal gold immunochromatographic strip (GICS) images with image processing algorithms is essential to quantitative analysis of GICS. As common methods for GICS image segmentation, fuzzy c-means (FCM) algorithm and cellular neural network (CNN) algorithm both require presetting initial conditions (specifying initial parameters or training models) and take long running time, due to high calculation cost. Therefore neither is ideal for a point-of-care testing (POCT) device, which has low hardware cost and limited computing power. This paper designs a region growing algorithm combined with fast peak detection (RGFPD) to quickly and self-adaptively segment GICS images. Compared with FCM algorithm and CNN algorithm, the RGFPD algorithm has two obvious advantages. First, as a local algorithm rather than a local one, the region growing algorithm requires low calculation cost, which better suits the POCT device. Second, the fast peak detection algorithm calculates the seed points and growing criterions as initial conditions, realizing self-adaptive segmentation of images. In this paper, RGFPD algorithm is applied to segment GICS images of actual samples, taking FCM algorithm and CNN algorithm as contrast. The results show that RGFPD accurately segment images without presetting initial conditions, with shorter algorithm running time, and performs better in anti-interference.

INDEX TERMS Colloidal gold immunochromatographic strip, image segmentation, peak detection, region growing, point-of-care testing.

I. INTRODUCTION

Point-of-care testing (POCT) is a significant development direction of modern laboratory medicine, see [1]–[3]. The gold immunochromatographic assay is one of the most widely used POCT technologies, due to its simple method, rapid reaction, low cost and good stability, see [4]–[8]. Accurate segmentation of test line (T Line) and control line (C Line) from the colloidal gold immunochromatographic strip (GICS) image is essential in quantitative analysis of GICS, [9], [10]. Fuzzy c-means (FCM) algorithm and cellular neural network (CNN) algorithm are two widely reported GICS image segmentation algorithms.

As one of the most widely used algorithms in unsupervised pattern recognition, FCM algorithm segments image via clustering pixels based on pixels attribute characteristics. Some authors in [11]–[16] have applied it to GICS image segmentation and achieved good results. However, initial parameters, such as the number of clusters and the weighting constant, has to be preset, and improper initial parameter settings will lower the segmentation effect. In addition, as a global algorithm, the FCM algorithm requires high calculation cost.

Inspired by the idea of cellular automata and neural networks, Chua and Yang in 1988 proposed cellular neural network [17], [18]. It is a large-scale nonlinear analog

The associate editor coordinating the review of this manuscript and approving it for publication was Carmelo Militello.

This work is licensed under a Creative Commons Attribution 4.0 License. For more information, see http://creativecommons.org/licenses/by/4.0/

algorithm that particularly suitable for complex systems, such as image processing, pattern recognition and artificial intelligence (AI). The self-adaptive learning ability enables CNN calculate the feedback template, control template and threshold template automatically by training a given sample set, without manually presetting initial parameters [17], [18]. Some authors in [19]–[21] have applied it to GICS image processing and obtained high precision segmentation result. However, it is not a self-adaptive algorithm in the real sense, because its self-adaptive learning modeling process is based on a given large amount of sample data. What's more, CNN algorithm requires higher calculation cost than FCM algorithm.

Both FCM algorithm and CNN algorithm can achieve ideal image segmentation effect on a powerful desktop computer. However, for POCT devices that are meant for fast detection, it is necessary to design a fast self-adaptive algorithm that requires low calculation cost and no preset initial conditions.

In order to lower the calculation cost so as to shorten the running time, this paper innovatively attempts to adopt region growing algorithm to segment GICS image. As a local algorithm, the region growing algorithm is easy to implement and produces excellent image boundary information and segmentation results [22], [23]. It has been widely used in segmenting CT and MRI images but scarcely applied in GICS image segmentation, see [24]–[27]. Compared with global algorithms like FCM and CNN, the region growing algorithm requires lower calculation cost. However, it also requires prespecifying appropriate seed points and growing criterions.

In order to avoid presetting initial conditions of the region growing algorithm, this paper designs a fast peak detection algorithm to quickly calculate the seed points and growing criterions. By integrating fast peak detection algorithm with region growing algorithm, this paper proposes region growing algorithm combined with fast peak detection (referred to as RGFPD) for GICS images segmentation. In order to evaluate its performance, RGFPD is applied to process a batch of GICS images of actual samples, taking FCM algorithm and CNN algorithm as contrast. The three algorithms are compared in aspects of image segmentation accuracy, algorithm running time, standard curve fitting and anti-interference ability.

II. CAPTURE OF GICS IMAGES

In this study, the vomitoxin (DON) is chosen as the analyte. 100uL of different concentration of DON solution (0, 1, 2.5, 5, 10, 20, 40ng/ml) is taken and added respectively to the sample pad of DON GICS in the same production batch (Wuhan NDH Biotechnology Company, Ltd). After the reaction, the strips are scanned with an optical scanner (EPSON PERFECTION V200 PHOTO) so as to capture the color GICS original images. The results are shown in Fig. 1.

III. DESIGN OF RGFPD ALGORITHM

Fig. 2 illustrates the implementation process of RGFPD, which consists of the following three steps:

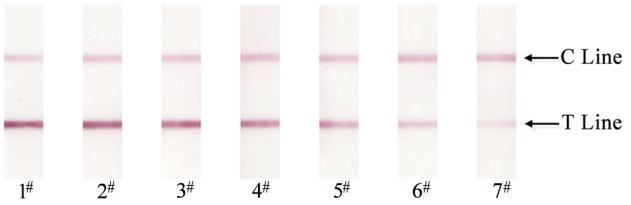

FIGURE 1. Images of colloidal gold immunochromatographic strip with different DON concentration (from $1^{\#}$ to $7^{\#}$: 0, 1, 2.5, 5, 10, 20, 40ng/ml).

i. The captured GICS original image is converted to gray image.
ii. The gray image is compressed, along the vertical direction of the GICS flow direction, into the one-dimensional Initial Curve. Via baseline correction, it is converted into the Corrected Curve, from which the seed points and growing criterions are calculated by extracting peak information.
iii. The binary image is formed by region growing of the gray image, with the seed point and growing criterions. Then the binary image is used as a mask to segment the C Line and T Line image from the gray image.

A. FAST PEAK DETECTION ALGORITHM

Peak detection algorithm is commonly used in chromatographic analysis, for it can quickly extract the peak information from a one-dimensional chromatographic curve, see [28]–[33]. In this paper, the GICS image is firstly compressed along the vertical direction of the GICS flow direction into a one-dimensional Initial Curve. Then a fast peak detection algorithm for calculation of the seed points and growing criterions is designed, using the chromatographic peak detection for reference. The specific implementation is as follows.

1) The gray image is compressed into one-dimensional Initial Curve via (1).

$$Y_i = (1/n) \times \sum_{j=1}^{n} U_{ij} (1 \le i \le m, 1 \le j \le n) \qquad (1)$$

where U is a gray image with m px × n px, U_{ij} is the gray-scale value of the pixel in the j-th column and the i-th row, Y_i is the ordinate value of the i-th point of the one-dimensional Initial Curve.

2) Baseline correction is performed on the Initial Curve as follow:

First, the Derivative Curve of the Initial Curve can be calculated by:

$$Z_i = \begin{cases} Y_{i+1} - Y_i \ (i = 1) \\ Y_i - Y_{i-1} \ (2 \le i \le m) \end{cases} \qquad (2)$$

where Z_i is the ordinate value of the i-th point of the Derivative Curve.

Second, the Derivative Curve is converted into the Square-wave Curve via (3). The starting and ending points of square wave in Square-wave Curve determine the starting

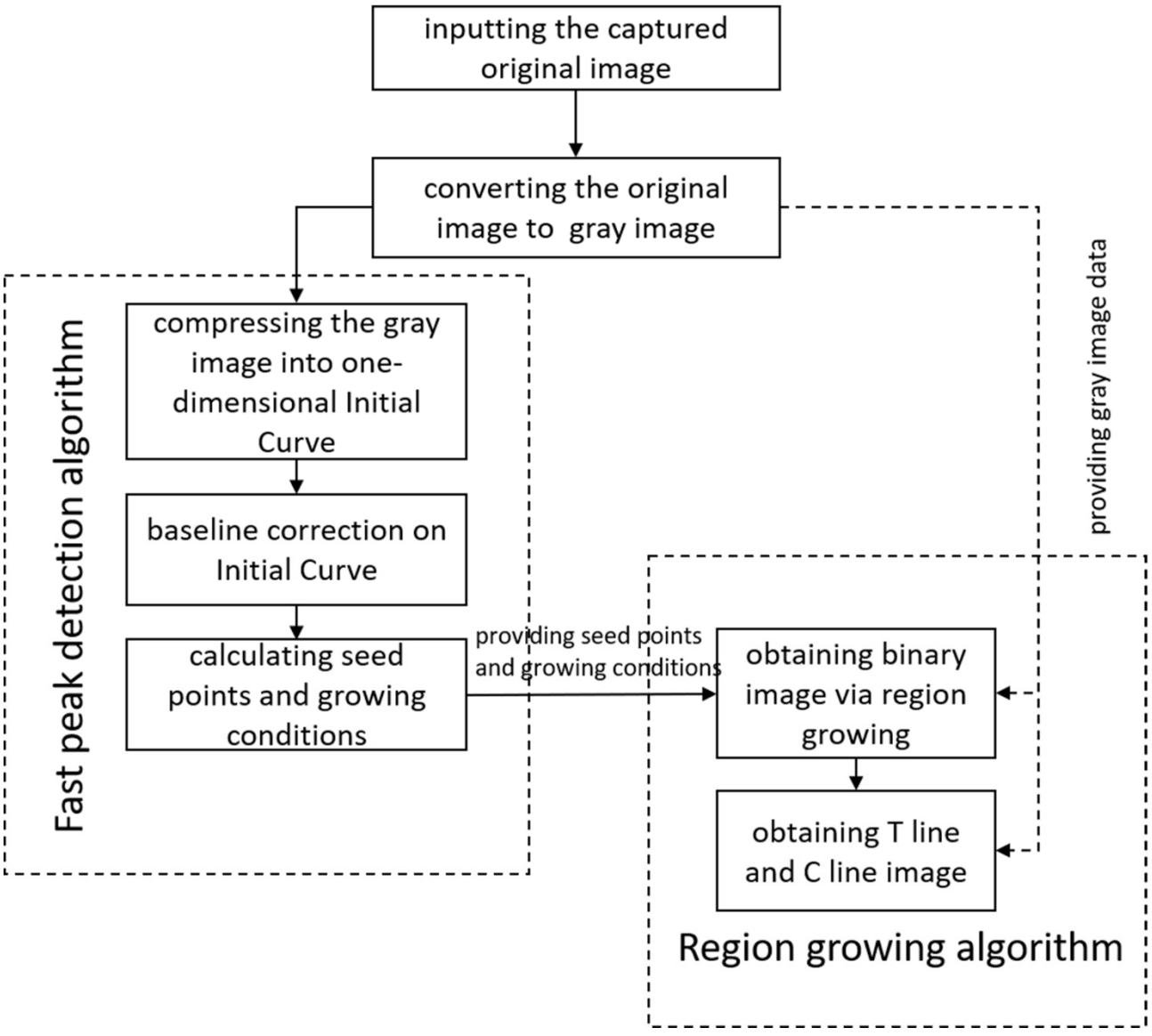

FIGURE 2. Flow chart of RGFPD algorithm.

and ending position (s_k and e_k, $k = 1, 2, \dots$) of peak in Initial Curve. The maximum value of k is corresponding to the number of square wave.

$$X_i = \begin{cases} 1\,(Z_i \geq a) \\ 0\,(-a < Z_i < a) \\ -1\,(Z_i \leq -a) \end{cases} \quad (1 \leq i \leq m) \tag{3}$$

where X_i is the ordinate value of the i-th point of the Square-wave Curve, a is one tenth of the maximum ordinate absolute value in the derivative curve. a is used to eliminate the noises in the Derivative Curve (This process is also called filtering).

Finally, according to s_k and $e_{k,}$, a continuous baseline is calculated by cutting off the peak from the Initial Curve and supplementing the missing part with linear interpolation. Then the Corrected Curve is obtained by subtracting the baseline from the Initial Curve. The detailed calculation of the Corrected Curve is shown in (4) (The maximum value of k is assumed to be 2).

$$C_i = \begin{cases} \dfrac{Y_{e_1} - Y_{s_1}}{e_1 - s_1} \times (i - s_1) - Y_i\,(s_1 \leq i \leq e_1) \\ \dfrac{Y_{e_2} - Y_{s_2}}{e_2 - s_2} \times (i - s_2) - Y_i\,(s_2 \leq i \leq e_2) \\ 0\,(1 \leq i < s_1 \cup e_1 < i < s_2 \cup e_2 < i \leq m) \end{cases} \tag{4}$$

where C_i is the ordinate value of the i-th point of the Corrected Curve, s_1, e_1, s_2, and e_2 are respectively the abscissa value of the starting point and the ending point of the first peak, and that of the second peak.

3) The peak information, including peak starting point abscissa value s_k, peak ending point abscissa value e_k, peak point abscissa value p_k, peak point ordinate value h_k, is extracted from the Corrected Curve, with which the seed points and growing criterions can be calculated. For the

convenience of discussion, the detailed calculations of the seed points and growing criterions are presented along with region growing algorithm.

B. REGION GROWING ALGORITHM COMBINED WITH FAST PEAK DETECTION

Region growing algorithm generally require artificially pre-specified seed points and growing criterions, which often leads to local optimization and fails to achieve the global optimal effect [22]. Therefore, the fast peak detection algorithm is adopted to self-adaptively calculate the seed points and growing criterions in this paper.

Calculation of seed points: The abscissa value p_k of each peak point in the Corrected Curve corresponds to the number of the row in which the seed point is located. In the p_k-th row of the gray image, the pixel point, whose gray-scale value is closest to the gray-scale average value of the row, is set as the seed point.

Calculation of growing criterions: 1). The growing threshold of each seed point is one third of its corresponding peak point ordinate value h_k. 2). The maximum region growing range of each seed point is s_k-th row to e_k-th row ($[s_k, e_k]$).

Using the seed points and growing criterions, region growing is performed on the gray image as shown in the following process, where the total number of pixel point of each row in the gray image is n, the region formed by region growing is named seed region (The initial seed region contains only the seed point), whereas the growing point is a pixel point that does not belong to the seed region within the growing range.

i. The initial value of seed region average gray-scale value Ga is set as the gray-scale value of seed point.
ii. Region growing is performed on the row where the seed points are located. If the difference between the gray-scale value of the growing point and Ga is less than the growing threshold, it is an effective growing point and will be merged into the seed region.
iii. After step 2, region growing will continue if the total number of pixel points in the formed seed region is greater than or equal to 70% of n. Otherwise, region growing will stop, with the existing growing result cleared and the region growing result reported blank.
iv. The value of Ga is updated by calculating the average gray-scale value of the newly formed seed region.
v. The seed region continues to grow outward (the upper row and next row), with the growing range controlled within $[s_k, e_k]$. If the difference between the gray-scale value of the growing point and Ga is less than the growing threshold, the growing point is effective and will be merged into the seed region. If no growing point is merged into the seed region, the region growing will stop, and the latest formed seed region will be output as the result.
vi. Define the total number of pixel points in the top row in the newly formed seed region as Tt, the total number in the bottom row as Tb. If both Tt$\geq$0.7$*$n and Tb$\geq$0.7$*$n, step 4 and 5 will repeat. If Tt$\geq$0.7$*$n and b$<$0.7$*$n, step 4 and 5 will continue, but the downward growing will stop. If Tt$<$0.7$*$n and Tb$\geq$0.7$*$n, step 4 and 5 will continue with the upward growing stopped. If both Tt$<$0.7$*$n and Tb$<$0.7$*$n, the region growing will stop with the latest formed seed region as output.

After all the seed points have completed region growing, the final result is formed by merging all region growing results, usually in the form of a binary image for better display, in which the white portion is the latest formed seed region. Using the binary image as a mask, the C Line and T Line image can be segmented from the gray image.

IV. EVALUATION OF RGFPD

Comprehensive evaluation of the RGFPD algorithm is conducted by analyzing its image segmentation accuracy, algorithm running time, standard curve fitting and anti-interference ability. Peak Signal to Noise Ratio (PSNR) is introduced for image segmentation evaluation, and the standard curve fitting requires quantitative calculation of GICS image.

A. EVALUATION OF GICS IMAGE SEGMENTATION RESULT

Peak Signal to Noise Ratio (PSNR) is adopted as standard to evaluate the accuracy of image segmentation [34]. The higher the PSNR value, the higher the accuracy. Firstly, a binary mask that classifies the pixels of GICS image as belonging to either signal (the T Line and C Line, which is assigned 0) or background (which is assigned 1) is produced. Then the PSNR can be calculated by:

$$\mathrm{PSNR} = 10 \times \lg\left[\frac{R^2}{MSE}\right] \tag{5}$$

where R is the maximum fluctuation in the input image data type. For example, if the data type of the input image is double-precision floating-point, R equals to 1. If the data type is an 8-bit unsigned integer, R equals to 255. MSE describes the cumulative squared error between the binary mask and the normalized gray image.

B. QUANTITATIVE CALCULATION OF GICS IMAGE

In order to quantitatively calculate the GICS system, the relative integral optical density (RIOD) based on the Beer-Lambert law is introduced to represent the concentration of the measured substance [34]. The RIOD is given as follows:

$$\mathrm{RIOD} = \frac{IOD_T}{IOD_C} = \frac{\sum_{i=1}^{N} lg\frac{G_0}{G_T^i}}{\sum_{j=1}^{M} lg\frac{G_0}{G_C^j}} \tag{6}$$

where $\mathrm{IOD_T}$ and $\mathrm{IOD_C}$ respectively describe the reflective integral optical density of the T Line and C Line. $\mathrm{G_T}$ and $\mathrm{G_C}$ denote the gray-scale value of pixel in the T Line and C Line. $\mathrm{G_0}$ represents the mean gray-scale value of the background in the reading window.

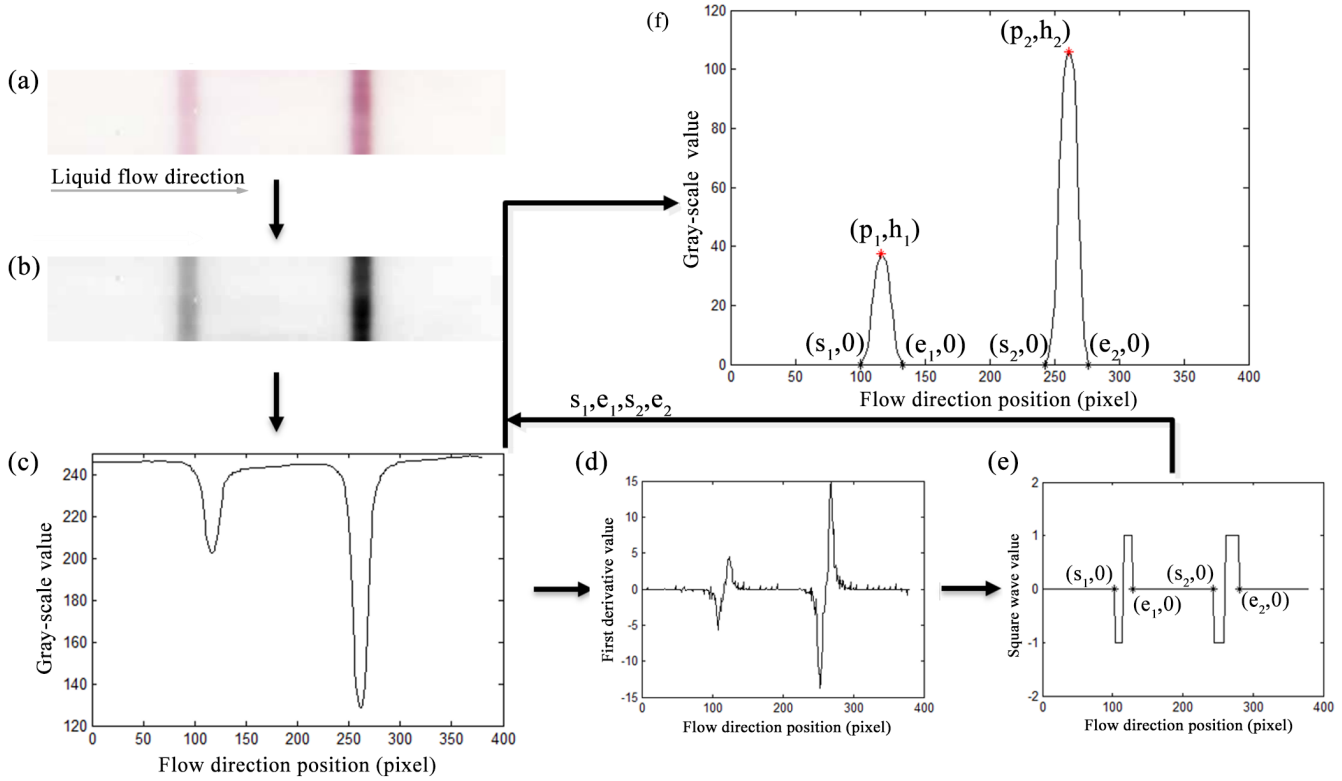

FIGURE 3. Result of fast peak detection. (a) The color GICS image (sample concentration is 2.5 ng/ml). (b) The gray image. (c) The Initial Curve. (d) The Derivative Curve. (e) The Square-wave Curve (s_k and e_k are the abscissa value of the starting and ending points of the square wave ($k = 1,2$)). (f) The Corrected Curve (s_k and e_k are the abscissa value of the starting and ending points of the peak. p_k and h_k are the abscissa value and ordinate value of peak point.)

V. RESULTS AND DISCUSSION

RGFPD, FCM, and CNN algorithms are adopted to process the same batch of GICS images, in order to compare their performance in aspects of image segmentation accuracy, algorithm running time, standard curve fitting and anti-interference ability. These algorithm programs are written in Matlab Version R2014a (The MathWorks, Inc.), and they run on a desktop computer with a 3.90 GHz Intel Core and 4.00 GB RAM on a Windows 10 operating system.

A. RESULT OF FAST PEAK DETECTION

The fast peak detection process of the GICS image with DON concentration of 2.5 ng/ml is shown in Fig. 3. First, the gray image (Fig. 3(b)) obtained by converting the color GICS image (Fig. 3(a)) is compressed by (1) to form the Initial Curve (fig. 3(c)). Second, the Initial Curve is computed into the Derivative Curve (Fig. 3(d)) by (2), which is then converted to the Square-wave Curve (fig. 3(e)) by (3). The starting and ending point of square wave determine the starting and ending position (s_k and e_k, $k = 1, 2$) of peak in Initial Curve. Third, according to s_k and e_k, the Corrected Curve (Fig. 3(f)) of Initial Curve is calculated by (4). Finally, The peak information of Corrected Curve is extracted for the seed points and growing criterions calculation, including peak starting point abscissa value s_k, peak ending point abscissa value e_k, peak point abscissa value p_k and peak point ordinate value h_k.

B. RESULT OF REGION GROWING

The region growing results of the GICS image with DON concentration of 2.5 ng/ml are shown in Fig. 4. First, with the peak information of Corrected Curve (Fig. 4(a)), the seed points and growing criterions are calculated. Then, region growing is performed on the gray image (Fig. 4(b)) to form the binary image (Fig. 4(c)). Finally, using the binary image as a mask, the T Line and C Line image (Fig. 3(d)) are segmented from the gray image. Comparing b and d, it can be observed that the algorithm proposed in this paper segments the T Line and C Line accurately.

C. COMPARISON OF ALGORITHM RUNNING TIME

RGFPD, FCM, and CNN algorithms are adopted to process the seven captured GICS images. Their running time are recorded and shown in Fig. 5.

FCM algorithm and CNN algorithm are global algorithms, whereas region growing algorithm is a local algorithm, which runs significantly faster than the other two. The fast peak detection algorithm also requires short running time. Therefore, the running time of RGFPD is significantly shorter than that of FCM and CNN. The average running time of RGFPD, FCM, and CNN are respectively 34.2ms, 331.6ms, and 882.6ms. RGFPD takes about 1/10 of FCM running time and 1/26 of CNN, which has obvious superiority in calculation cost.

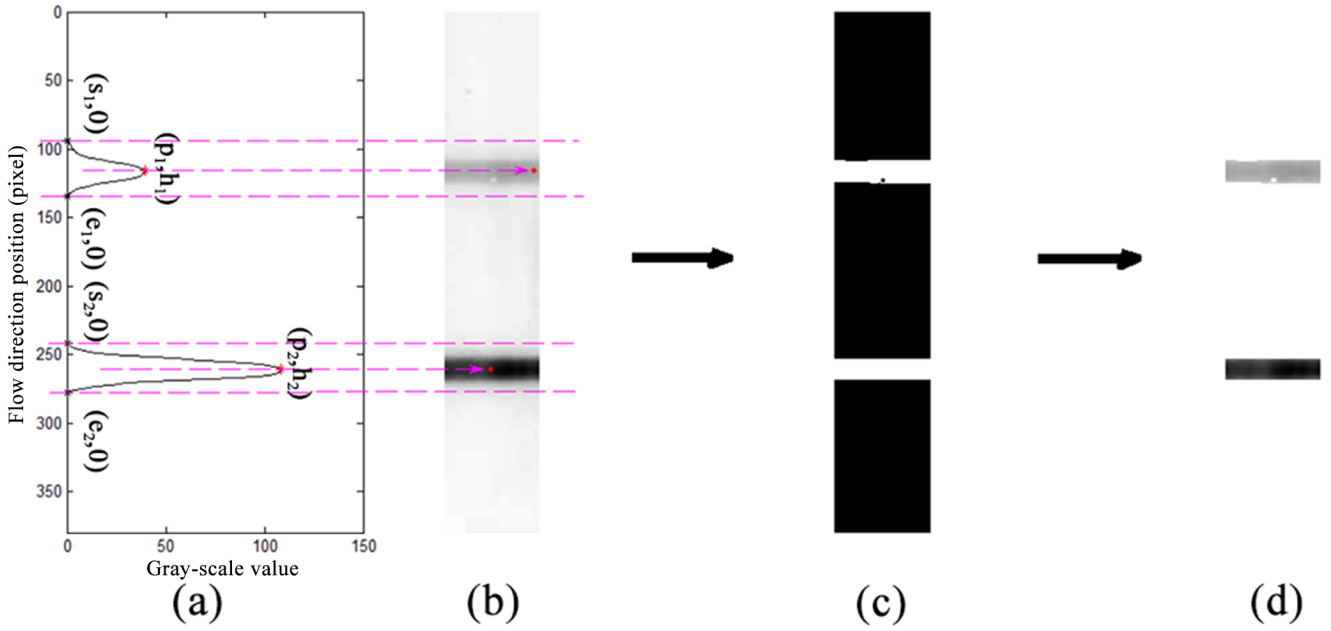

FIGURE 4. Result of region growing. (a) The Corrected Curve. (b)The gray image with the seed points. (c) The binary image. (d) The T Line and C Line image.

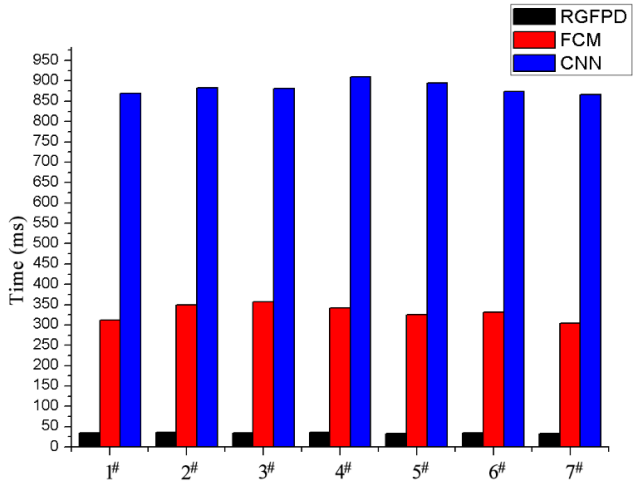

FIGURE 5. Algorithm running time of RGFPD, FCM and CNN. 1# to 7# corresponds to GICS images with different DON concentration.

D. COMPARISON OF IMAGE SEGMENTATION ACCURACY

The PSNR is introduced to evaluate the image segmentation accuracy of RGFPD, FCM, and CNN for seven captured GICS images. Their PSNR are calculated by (5) and shown in Table 1.

Taking running time and PSNR value into consideration, we can conclude that: i. CNN has the longest running time but the highest image segmentation accuracy. ii. RGFPD achieves similar image segmentation accuracy with only 1/26 of CNN running time. iii. FCM has the lowest image segmentation accuracy.

E. STANDARD CURVE FITTING

The standard curve fitting is the basis for quantitative analysis. First, RGFPD, FCM, and CNN algorithms are adopted to segment six of the acquired GICS images of known DON concentrations (concentrations: 1, 2.5, 5, 10, 20, 40 ng/m). With their respective RIOD calculated by (6), the curve fitting of RIOD and DON concentration are performed by logical four-parameter fitting method. The results are shown in Fig. 6.

As indicated in Fig. 6, good corresponding relationship is seen between RIOD and DON concentration in GICS images segmentation via RGFPD. The correlation coefficient of RGFPD reached 0.999, slightly higher than that of FCM 0.998, and 0.995 of CNN. It shows that RGFPD segmentation result achieve better effect of curve fitting, which will serve quantitative analysis of GICS images.

F. COMPARISON OF SEGMENTATION RESULTS OF GICS IMAGES WITH INTERFERENCE

In practical applications, GICS samples with interference, such as noise point, water traces and shadow, are often captured, due to uneven illumination and improper operation. In the actual test, RGFPD exhibits good anti-interference ability. In this section, RGFPD, FCM and CNN are utilized to process four GICS images with different interference. The image segmentation results are shown in Fig. 7.

We can conclude from Fig.7 that RGFPD has stronger anti-interference ability than FCM and CNN. One reason is that RGFPD filters some noise during the fast peak detection, eliminating some small-area interference, such as large noise points and small sundries. Another is that RGFPD sets effective growing-stop conditions in the process of region growing, which eliminates some large-area interference, such as large-area water traces and large-area shadow.

TABLE 1. PSNR values of RGFPD, FCM, and CNN.

PSNR	RGFPD	FCM	CNN
Image 1	18.49	15.96	18.64
Image 2	18.45	16.20	18.57
Image 3	17.93	16.41	18.03
Image 4	16.33	15.68	16.47
Image 5	16.58	15.17	16.95
Image 6	17.33	17.31	17.42
Image 7	15.65	14.45	16.06

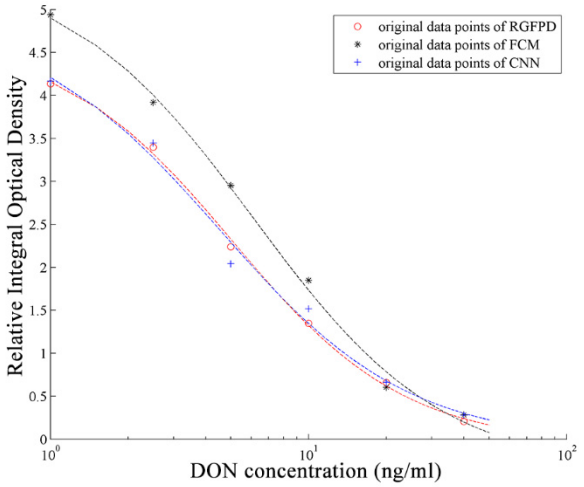

FIGURE 6. Curve of RIOD and DON concentration.

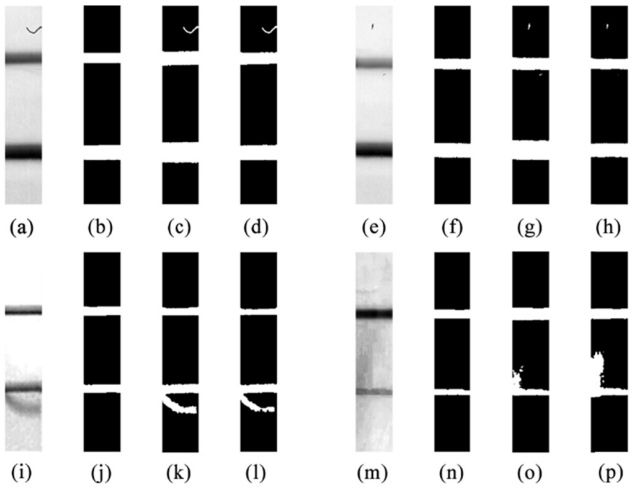

FIGURE 7. Results of processing the GICS images with interference via RGFPD, FCM and CNN. (a), (e), (i) and (m) The GICS gray image with sundries, large noise, water traces and shadow, respectively. (b), (f), (j), (n)Corresponding results by RGFPD.(c), (g), (k), (o)Corresponding results by FCM. (d), (h), (l), (p)Corresponding results by CNN.

VI. CONCLUSION

POCT technology has drawn growing concern in modern trend of diagnosis-and-treatment integration and personalized medicine [35], [36]. Although the existing PC-based graphics processing algorithms achieve adequate accuracy, it is too complex to be fully applicable to POCT devices with low cost and limited computing power. In this paper, a fast and self-adaptive RGFPD algorithm is proposed for GICS image segmentation. First, in order to lower the calculation cost, the region growing algorithm, a local algorithm, is adopted for image segmentation algorithm. Then, in order to avoid the initial conditions preset of the region growing algorithm, a fast peak detection algorithm is designed to calculate the seed points and growing criterions.

In order to evaluate the RGFPD algorithm, two commonly used GICS image segmentation methods (FCM algorithm and CNN algorithm) are selected as contrast. RGFPD, FCM, and CNN are compared in perspectives of image segmentation accuracy, algorithm running time, standard curve fitting and anti-interference ability. The results show that RGFPD has three advantages. First, the region growing algorithm is adopted as the image segmentation method that requires lower calculation cost. RGFPD shortens the running time by over 90%, compared to FCM and CNN. Second, a fast peak detection algorithm is utilized to calculate the seed points and growing criterions required by region growing, which not only avoids the image segmentation deviation caused by the unreasonable conditions setting, but also require no learning modeling process, realizing self-adaptive segmentation of GICS images.

Meanwhile, RGFPD has better anti-interference ability in the process of segmenting GICS images. On the one hand, RGFPD includes a filtering process that eliminates some small-area interference before region growing. On the other hand, by setting effective growing-stop conditions, some large-area interference is avoided during region growing. Therefore, when segmenting GICS images with interference, RGFPD acquires more accurate result than FCM and CNN algorithms.

In this paper, for the first time, the region growing algorithm is applied to greatly shorten the GICS segmentation time. What's more, by combining the fast peak detection algorithm, the region growing algorithm avoid manual set of initial conditions, such as seed points and growing criterions, realizing the real self-adaptivity. However, this algorithm has some limitations. If the interference area is large and the width is close to the width of the strip, the RGFPD algorithm may not be able to accurately distinguish the interference.

If an obvious fault exists in the C Line or T Line signal, under-segmentation may occur. In addition, the RGFPD algorithm is only studied and applied based on GICS images, the application of which in fluorescent labeling immunochromatography, dot gold immunochromatography and other fields is yet to be expanded.

ACKNOWLEDGMENT

The authors would like to thank the HUST Analytical and Testing Center for allowing us to use its facilities.

The demo software of RGFPD (for 64 bits Windows system only) is available free of charge on the website at http://112.124.106.109/RGFPD_DEMO.ZIP.

(Wensheng Guo and Yue Zhang contributed equally to this work).

REFERENCES

[1] J. Yang, K. Wang, H. Xu, W. Yan, Q. Jin, and D. Cui, "Detection platforms for point-of-care testing based on colorimetric, luminescent and magnetic assays: A review," *Talanta*, vol. 202, pp. 96–110, Sep. 2019.

[2] Q. Qin, K. Wang, J. Yang, H. Xu, B. Cao, Y. Wo, Q. Jin, and D. Cui, "Algorithms for immunochromatographic assay: Review and impact on future application," *Analyst*, vol. 144, no. 19, pp. 5659–5676, 2019, doi: 10.1039/c9an00964g.

[3] D. Lingervelder, H. Koffijberg, R. Kusters, and M. J. IJzerman, "Point-of-care testing in primary care: A systematic review on implementation aspects addressed in test evaluations," *Int. J. Clin. Pract.*, vol. 73, no. 10, 2019, Art. no. e13392, doi: 10.1111/ijcp.13392.

[4] M. Sajid, A.-N. Kawde, and M. Daud, "Designs, formats and applications of lateral flow assay: A literature review," *J. Saudi Chem. Soc.*, vol. 19, no. 6, pp. 689–705, Nov. 2015.

[5] K. Omidfar, F. Khorsand, and M. D. Azizi, "New analytical applications of gold nanoparticles as label in antibody based sensors," *Biosensors Bioelectron.*, vol. 43, pp. 336–347, May 2013.

[6] S.-H. Paek, J.-H. Cho, I.-H. Cho, Y.-K. Kim, and B.-K. Oh, "Immunosensors for point-of-care testing," *Biochip J.*, vol. 1, no. 1, pp. 1–16, Mar. 2007.

[7] B. Zhang, W. Ma, F. Li, W. Gao, Q. Zhao, W. Peng, J. Piao, X. Wu, H. Wang, X. Gong, and J. Chang, "Fluorescence quenching-based signal amplification on immunochromatography test strips for dual-mode sensing of two biomarkers of breast cancer," *Nanoscale*, vol. 9, no. 47, pp. 18711–18722, Dec. 2017.

[8] Y. Yao, W. Guo, J. Zhang, Y. Wu, W. Fu, T. Liu, X. Wu, H. Wang, X. Gong, X.-J. Liang, and J. Chang, "Reverse fluorescence enhancement and colorimetric bimodal signal readout immunochromatography test strip for ultrasensitive large-scale screening and postoperative monitoring," *ACS Appl. Mater. Interfaces*, vol. 8, no. 35, pp. 22963–22970, Sep. 2016.

[9] S. Ghosh and C. H. Ahn, "Lyophilization of chemiluminescent substrate reagents for high-sensitive microchannel-based lateral flow assay (MLFA) in point-of-care (POC) diagnostic system," *Analyst*, vol. 144, no. 6, pp. 2109–2119, Mar. 2019.

[10] C.-S. Lin, C.-Y. Wu, H.-C. Hsu, K.-M.-C. Li, and L. Lin, "Rapid bio-test strips reader with image processing technology," *Optik*, vol. 115, no. 8, pp. 363–369, Aug. 2004.

[11] J. Liu, Z. Kong, Y. Wang, Y. Fan, J. Luo, S. Xu, H. Jin, and X. Cai, "A rapid quantitative determination method of luteinizing hormone with gold immunochromatographic strip," in *Proc. EMBC*, Jeju-do, South Korea, 2017, pp. 17–20.

[12] Y. Wu, Y. Gao, and M. Du, "Quantitative detection of the colloidal gold immunochromatographic strip in HSV color space," *Proc. SPIE*, vol. 9282, Sep. 2014, Art. no. 928231, doi: 10.1117/12.2068033.

[13] J. Zhang and M. Du, "Fast image segmentation of gold immunochromatographic strip based on FCM clustering algorithm in HSV color space," in *Proc. CISP*, Chongqing, China, 2012, pp. 525–528.

[14] J. Liu, Y. Fan, Z. Kong, Y. Wang, J. Luo, S. Xu, H. Jin, and X. Cai, "Smartphone-based rapid quantitative detection of luteinizing hormone using gold immunochromatographic strip," *Sens. Actuators B, Chem.*, vol. 259, pp. 1073–1081, Apr. 2018.

[15] Y.-M. Gao, J.-C. Wei, P.-U. Mak, M.-I. Vai, M. Du, and S.-H. Pun, "Development of a calibration strip for immunochromatographic assay detection systems," *Sensors*, vol. 16, no. 7, p. 1007, Jul. 2016.

[16] N. Zeng, Y. Li, and M. Du, "Rapid quantitative image analysis of hCG by gold immunochromatographic assay and genetic fast FCM algorithm," in *Proc. BMEI*, Yantai, China, 2010, pp. 1560–1564.

[17] L. O. Chua and L. Yang, "Cellular neural networks: Applications," *IEEE Trans. Circuits Syst.*, vol. CAS-35, no. 10, pp. 1273–1290, Oct. 1988.

[18] L. O. Chua and L. Yang, "Cellular neural networks: Theory," *IEEE Trans. Circuits Syst.*, vol. CAS-35, no. 10, pp. 1257–1272, Oct. 1988.

[19] N. Zeng, Y. You, L. Xie, H. Zhang, L. Ye, W. Hong, and Y. Li, "A new imaged-based quantitative reader for the gold immunochromatographic assay," *Optik*, vol. 152, pp. 92–99, Jan. 2018.

[20] N. Zeng, Z. Wang, B. Zineddin, Y. Li, M. Du, L. Xiao, X. Liu, and T. Young, "Image-based quantitative analysis of gold immunochromatographic strip via cellular neural network approach," *IEEE Trans. Med. Imag.*, vol. 33, no. 5, pp. 1129–1136, May 2014.

[21] B. Zineddin, Z. Wang, Y. Shi, Y. Li, M. Du, and X. Liu, "A multi-view approach to cDNA micro-array analysis," *Int. J. Computat. Biol. Drug Des.*, vol. 3, no. 2, pp. 91–111, Sep. 2010.

[22] S. A. Hojjatoleslami and J. Kittler, "Region growing: A new approach," *IEEE Trans. Image Process.*, vol. 7, no. 7, pp. 1079–1084, Jul. 1998.

[23] Y. Deng and B. S. Manjunath, "Unsupervised segmentation of color-texture regions in images and video," *IEEE Trans. Pattern Anal. Mach. Intell.*, vol. 23, no. 8, pp. 800–810, Aug. 2001.

[24] D. Chen, M. R. Wax, L. Li, Z. Liang, B. Li, and A. E. Kaufman, "A novel approach to extract colon lumen from CT images for virtual colonoscopy," *IEEE Trans. Med. Imag.*, vol. 19, no. 12, pp. 1220–1226, Dec. 2000.

[25] J. Dehmeshki, H. Amin, M. Valdivieso, and X. Ye, "Segmentation of pulmonary nodules in thoracic CT scans: A region growing approach," *IEEE Trans. Med. Imag.*, vol. 27, no. 4, pp. 467–480, Apr. 2008.

[26] V. Schulz, I. Torres-Espallardo, S. Renisch, Z. Hu, N. Ojha, P. Börnert, M. Perkuhn, T. Niendorf, W. M. Schäfer, H. Brockmann, T. Krohn, A. Buhl, R. W. Günther, F. M. Mottaghy, and G. A. Krombach, "Automatic, three-segment, MR-based attenuation correction for whole-body PET/MR data," *Eur. J. Nucl. Med. Mol. Imag.*, vol. 38, no. 1, pp. 138–152, Jan. 2011.

[27] P. A. Freeborough, N. C. Fox, and R. I. Kitney, "Interactive algorithms for the segmentation and quantitation of 3-D MRI brain scans," *Comput. Methods Programs Biomed.*, vol. 53, no. 1, pp. 15–25, May 1997.

[28] L. D. Asnin, "Peak measurement and calibration in chromatographic analysis," *TrAC Trends Anal. Chem.*, vol. 81, pp. 51–62, Jul./Aug. 2016.

[29] M. G. Knize, J. S. Felton, and G. A. Gross, "Chromatographic methods for the analysis of heterocyclic amine food mutagens/carcinogens," *J. Chromatogr.*, vol. 624, nos. 1–2, pp. 253–265, Oct. 1992.

[30] C. A. Smith, E. J. Want, G. O'Maille, R. Abagyan, and G. Siuzdak, "XCMS: Processing mass spectrometry data for metabolite profiling using Nonlinear peak alignment, matching, and identification," *Anal. Chem.*, vol. 78, no. 3, pp. 779–787, Feb. 2006.

[31] M. Katajamaa and M. Oresic, "Data processing for mass spectrometry-based metabolomics," *J. Chromatogr. A*, vol. 1158, nos. 1–2, pp. 318–328, Jul. 2007.

[32] Z.-M. Zhang, S. Chen, and Y.-Z. Liang, "Baseline correction using adaptive iteratively reweighted penalized least squares," *Analyst*, vol. 135, no. 5, pp. 1138–1146, Feb. 2010.

[33] J. Yang, X. Zhao, X. Liu, C. Wang, P. Gao, J. Wang, L. Li, J. Gu, S. Yang, and G. Xu, "High performance liquid chromatography-mass spectrometry for metabonomics: Potential biomarkers for acute deterioration of liver function in chronic hepatitis B," *J. Proteome Res.*, vol. 5, no. 3, pp. 554–561, Mar. 2006.

[34] Y. Li, N. Zeng, and M. Du, "A novel image methodology for interpretation of gold immunochromatographic strip," *J. Comput.*, vol. 6, no. 3, pp. 540–547, Mar. 2011.

[35] J. Liu, Z. Geng, Z. Fan, J. Liu, and H. Chen, "Point-of-care testing based on smartphone: The current state-of-the-art (2017–2018)," *Biosensors Bioelectron.*, vol. 132, pp. 17–37, May 2019.

[36] H. Kim, D.-R. Chung, and M. Kang, "A new point-of-care test for the diagnosis of infectious diseases based on multiplex lateral flow immunoassays," *Analyst*, vol. 144, no. 8, pp. 2460–2466, Apr. 2019.

WENSHENG GUO was born in Hubei, China, in 1995. He received the bachelor's degree in medical imaging engineering from the Department of Medical Instrument and Food Engineering, University of Shanghai for Science and Technology, Shanghai, China, in 2016. He is currently pursuing the Ph.D. degree in biopharmaceutical engineering with the Huazhong University of Science and Technology. His research interests include medical image processing and pattern recognition.

YUE ZHANG was born in Sichuan, China, in 1979. She received the B.A. degree in English, with a focus on English for Science and Technology (EST) and the M.A. degree in foreign linguistics and applied linguistics from the Huazhong University of Science and Technology (HUST), Wuhan, Hubei, China, in 2001 and 2004. She is currently a Lecturer with the School of Engineering Sciences, Wuhan National Laboratory for Optoelectronics, HUST.

XIAOYAN HU, photograph and biography not available at the time of publication.

TING ZHANG, photograph and biography not available at the time of publication.

MING LIANG, photograph and biography not available at the time of publication.

XIANGLIANG YANG, photograph and biography not available at the time of publication.

HAI YANG was born in Hunan, China, in 1977. He received the B.S. degree in chemical engineering and the Ph.D. degree environmental engineering from the Huazhong University of Science and Technology, Wuhan, China, in 2000 and 2006, respectively.

He is currently a Lecturer of biomedical engineering with the Huazhong University of Science and Technology. His research has been concerned with nanoparticles labeled point-of-care testing and portable analyzer.

Dr. Yang is also the Director of Wuhan Key Laboratory of Nano-diagnostics and Analytical Technology for Biomedicine and the Head of the Nano-Diagnostic Agent Department, National Engineering Research Center for Nanomedicine of China.